The Astrophysical Journal, 655:606–614, 2007 January 20

A STATISTICAL STUDY OF SHEAR MOTION OF THE FOOTPOINTS IN TWO-RIBBON FLARES

Yingna Su,[1,2] Leon Golub,[2] and Adriaan A. Van Ballegooijen[2]
Received 2006 September 13; accepted 2006 October 9

ABSTRACT

We present a statistical investigation of shear motion of the ultraviolet (UV) or extreme-ultraviolet (EUV) footpoints in two-ribbon flares, using the high spatial resolution data obtained in 1998–2005 by *TRACE*. To do this study, we have selected 50 well-observed X and M class two-ribbon flares as our sample. All 50 of these flares are classified into three types based on the motions of the footpoints with respect to the magnetic field (*SOHO* MDI). The relation between our classification scheme and the traditional classification scheme (i.e., "ejective" and "confined" flares) is discussed. We have found that 86% (43 out of 50) of these flares show both strong-to-weak shear change of footpoints and ribbon separation (type I flares), and 14% of the flares show no measurable shear change of conjugate footpoints, including two flares with very small ribbon separation (type II flares) and five flares having no ribbon separation at all through the entire flare process (type III flares). Shear motion of footpoints is thus a common feature in two-ribbon flares. A detailed analysis of the type I flares shows (1) for a subset of 20 flares, the initial and final shear angles of the footpoints are mainly in the range 50°–80° and 15°–55°, respectively; and (2) in 10 of the 14 flares having both measured shear angle and corresponding hard X-ray observations, the cessation of shear change is 0–2 minutes earlier than the end of the impulsive phase, which may suggest that the change from impulsive to gradual phase is related to magnetic shear change.

Subject headings: Sun: corona — Sun: flares — Sun: magnetic fields — Sun: UV radiation

1. INTRODUCTION

Solar flares can be grouped according to the number of ribbons, from unresolved compact pointlike flares to four-ribbon flares. The most commonly seen chromospheric flare morphology is the two-ribbon flare, according to Tang (1985). It is well known that ribbons of large two-ribbon flares separate as a function of time. This ribbon separation is interpreted as the chromospheric signature of the progressive magnetic reconnection in the corona, in which new magnetic field lines reconnect at higher and higher altitudes, according to the two-dimensional classical "CSHKP" model for two-ribbon flares (Svestka & Cliver 1992).

After analyzing 31 flares observed by the Hard X-Ray telescope (HXT) on board *Yohkoh*, Bogachev et al. (2005) classified the footpoint motions into three types: (1) motion away from and nearly perpendicular to the magnetic inversion line (MIL) (ribbon separation), (2) motion mainly along the MIL and in antiparallel directions (shear motion), and (3) parallel motion in the same direction along the MIL. Furthermore, they found that 14 out of their 31 flares show the second type of motion, which often appears as strong-to-weak shear change of the footpoints during a flare. This shear motion was also found in several individual two-ribbon flares (Ji et al. 2006; Su et al. 2006, hereafter Paper I, and references therein). This motion cannot be explained by a simplified two-dimensional flaring model, but it is instead consistent with a three-dimensional magnetic field configuration having highly sheared inner and less sheared outer magnetic field lines in the preflare phase (Moore et al. 1995 and references therein). The cessation of shear change during the impulsive phase can be interpreted as a splitting of the envelope of the highly sheared core field, according to Paper I.

So far, this change from strong to weak shear of the footpoints during the flare has been reported in almost 20 solar flares, which suggests that this motion may be a common feature in solar flares. In this paper we have made a detailed statistical study of the shear motion of the footpoints in 50 two-ribbon flares using high spatial resolution extreme-ultraviolet (EUV)/ultraviolet (UV) images obtained with the *Transition Region and Corona Explorer* (*TRACE*; Handy et al. 1999), in order to make a conclusive statement about the prevalence of shear motion of footpoints in such flares. Our flares are classified into three groups: type I flares, which show both ribbon separation and shear motion; type II flares, which show only ribbon separation; and type III flares, which show no footpoint motion.

It is often considered that, to a first approximation, the life history of a flare consists of an impulsive phase, characterized by mainly nonthermal emissions (hard X-rays, gamma rays, radio waves, and neutrons) and a gradual (main) phase characterized by predominantly thermal emissions (soft X-rays, UV, and optical radiation; Tandberg-Hanssen & Emslie 1988). The impulsive and gradual phases can also be recognized on the basis of hard X-ray (HXR) and microwave time profiles. The impulsive emissions have a short timescale, of order several tens of seconds to a few minutes, and gradual emissions evolve over a longer timescale of tens of minutes. The distinction between the two turns out to be more than superficial and is not limited to temporal properties. Statistical and case studies in the last two decades revealed other respects in which the impulsive and gradual emissions show contrasting properties (for a detailed review see Qiu et al. 2004 and references therein).

The physical differences between the flare impulsive phase and gradual phase are pronounced, and the transition from impulsive phase to main phase is typically abrupt. What is the nature of the change that occurs when a flare goes from the impulsive phase to the gradual phase? The magnetic field strength per se is unlikely to change abruptly, but the magnetic shear may show abrupt temporal gradients. Therefore, Lynch et al. (2004) suggested that the observed cessation of HXR bursts with the start of the main phase can be understood in terms of the difference between reconnection in a strongly sheared versus an unsheared

[1] Purple Mountain Observatory, Nanjing, China; and Graduate University of Chinese Academy of Sciences, China.
[2] Current address: Harvard-Smithsonian Center for Astrophysics, Cambridge, MA; ynsu@head.cfa.harvard.edu.

field. This hypothesis has been examined in detail for one flare in our previous paper (Paper I). The observations showed that the cessation of shear change of footpoints occurs in the middle of the impulsive phase. However, it is difficult to draw a conclusive statement on this question from this one case study. In this paper we examine the time difference between the cessation of the shear motion and the end of the impulsive phase in a sample of 14 events having both measurable shear angle and corresponding HXR observations.

The observational data are summarized in § 2. In § 3.1 we present the study of type I flares. The observational results of type II and III flares are described in § 3.2. In §§ 4.1 and 4.2 we compare our classification scheme (type I, II, and III flares) with that of Svestka (1986) ("ejective" and "confined" flares), and an energy scale for two-ribbon flares is described in § 4.3. The time difference between the cessation of shear motion and the end of impulsive phase in type I flares is presented in § 5. Summary is given in § 6.

2. OBSERVATIONAL DATA

We construct our data sets based on the *TRACE* Flare Catalog,[3] provided by the Solar and Stellar X-Ray Group at Smithsonian Astrophysical Observatory, which lists all of those X and M class flares (*GOES* soft X-ray) from 1998 May to the present time (and those C class flares from 1998 to 2002, and they are not cataloged after this) observed by *TRACE*. The *TRACE* Flare Catalog is formed by selecting those flare events having *TRACE* observations around the flare peak time reported by *GOES*. The information of the class and peak time of the flares listed in the *TRACE* Flare Catalog is taken from the *GOES* Flare Catalog.[4] We have selected 50 well-observed two-ribbon solar flares from 1998 to 2005, according to the following criteria:

1. We only consider flares in which two long and roughly parallel ribbons are seen during the flare.
2. Most parts of the two ribbons are visible within the field of view (FOV) of *TRACE*.
3. *TRACE* obtained several good images during the rise and impulsive phase, from which we can see the two ribbons and their evolution clearly.
4. Flares near the limb for which the two ribbons and their evolution cannot be seen are not considered.

All of the flares we included in this study are listed in Tables 1 and 2.

The *TRACE* mission explores the dynamics and evolution of the solar atmosphere from the photosphere to the corona with high spatial and temporal resolution (Handy et al. 1999). It observes the white-light photosphere, the transition region at the wavelengths of 1216, 1550, and 1600 Å, and the 1–2 MK corona at 171, 195, and 284 Å. However, because of its limited FOV, *TRACE* may miss observing some flares, if these flares happen outside the FOV (Zhang et al. 2002). We have used the *TRACE* catalog, understanding that it will not be a complete sample of all flares occurring during the studied period because the *TRACE* observations of flares provide high spatial and temporal resolution images, which make possible the study of shear motion of the footpoints.

The HXR time profiles used in this study from 1998 to 2001 are taken from the *Yohkoh* Flare Catalog.[5] *Yohkoh* HXT (Kosugi et al. 1991) used a Fourier synthesis technique to take images in four energy bands (L: 13–23 keV; M1: 23–33 keV; M2: 33–53 keV; H: 53–93 keV) with a collimator response (FWHM) of about 8″. For those flares that occurred after 2001, the HXR data are obtained from *RHESSI*. *RHESSI* provides unprecedented high-resolution imaging and spectroscopy capability for solar flares (Lin et al. 2002). For the analysis, we use the energy band 33–53 keV for both *Yohkoh* HXT and *RHESSI*, since lower energy bands may have a considerable contribution from the superhot plasma emission. We could also use a higher energy band, but the HXR emission is usually too weak in those bands to define the end of the impulsive phase with proper accuracy.

The magnetic inversion line information in most events used in this study is from the line-of-sight photospheric magnetograms observed by the Michelson Doppler Imager (MDI) on board the *Solar and Heliospheric Observatory* (*SOHO*). For those events that do not have corresponding MDI observations, or if the MIL on the MDI magnetograms is too complicated, the MIL is identified by the corresponding filament on the Hα images observed by Big Bear Solar Observatory (BBSO). Information about related coronal mass ejections (CMEs) is obtained from the *SOHO* Large Angle and Spectrometric Coronagraph Experiment (LASCO) CME Catalog.[6]

3. THREE TYPES OF TWO-RIBBON FLARES

Of the available *TRACE* passbands, more than half of the events we studied were mainly observed only in the EUV (171/195 Å) or UV (1600/1700 Å), and less than half of them were observed with a sequence that took a combination of EUV (171/195/284 Å) and UV (1600/1216/1550 Å) images. In order to study shear motion of the footpoints, our first step is to look through all of the movies at the wavelength in the main observing sequence for each event, i.e., the wavelength that has the best coverage of the event. The motion of the brightenings can be seen clearly from the movies and is visible in either UV or EUV channels. To make a detailed study, we first synthesized a set of *TRACE* images at the wavelength in main observing sequence for each event. In order to distinguish the motions of footpoints with respect to the magnetic field, the next step is to co-align the *TRACE* images with the corresponding magnetic field or Hα images. To get good co-alignment of the EUV/UV (*TRACE*) and *SOHO* MDI magnetograms or BBSO Hα image, we proceeded in three steps: (1) aligned the EUV/UV images with the white-light (WL) images observed by *TRACE* using the "trace_prep.pro" program provided as part of the *TRACE* analysis software; (2) aligned the WL images with the *SOHO* MDI magnetograms or BBSO Hα images, using the dark sunspots; (3) aligned the EUV/UV images with the *SOHO* MDI images or BBSO Hα images using the offsets obtained from the first two steps.

After studying the motions of the brightenings observed by *TRACE* with respect to the magnetic field, we found that our events could be categorized into three groups:

Type I flares.—The common characteristic among all flares in this group is that the EUV conjugate footpoints start at a position close to the magnetic inversion line but widely separated along the MIL (highly sheared) and change into a configuration far from and straight across the inversion line (less sheared) during the impulsive phase. In other words, this type of flare shows strong-to-weak shear motion of the footpoints and also ribbon separation.

An example of a type I flare on 2001 April 26 is shown in Figure 1. Figure 1*a* represents the HXR time profiles obtained from *Yohkoh* HXT. The *TRACE* EUV initial brightenings (*white contours*) at the flare onset overlaid on the EUV image having the final brightenings at the time when the shear change stops are

[3] See http://hea-www.harvard.edu/trace/flare_catalog/.
[4] See http://www.lmsal.com/SXT/plot_goes.html.
[5] See http://gedas22.stelab.nagoya-u.ac.jp/HXT/catalogue/index.html.
[6] See http://cdaw.gsfc.nasa.gov/CME_list/index.html.

TABLE 1
TYPE I FLARES WITH SHEAR MOTION AND RIBBON SEPARATION

DATE	*GOES* CLASS	*TRACE* OBSERVED BAND(S) (Å)	*TRACE* SHEAR ANGLE θ_1[a] (deg)	θ_2[a] (deg)	$\theta_1 - \theta_2$ (deg)	TIME t_{EUV1}[b] (UT)	t_{EUV2}[b] (UT)	t_{HXR}[c] (UT)	$t_{HXR} - t_{EUV2}$ (s)	*GOES* Peak (UT)	CME ONSET (UT)
1998 Sep 23	M7.1	1550, 195	...	...	...	...	...	...	...	07:13	No data
1999 Jun 22	M1.7	1216, 195, 171	52±2	31±2	21	18:20:26	18:24:51	18:23	−111	18:29	18:54
1999 Jun 23	M1.7	1216, 195, 171	56±2	32±2	24	06:50:42	06:57:02	...	...	07:09	07:31
2000 Feb 08	M1.3	171, 1600	65±2	19±2	46	08:44:05	08:49:32	08:51:55	143	09:00	09:30
2000 Apr 12	M1.3	171	...	...	...	...	...	...	...	03:35	No
2000 Jun 04	M3.2	171, 1600	67±2	49±2	16	22:06	22:09:27	...	...	22:10	23:54
2000 Jun 06	X2.3	171, 1600	...	...	...	...	...	...	...	15:25	15:30
2000 Jun 10	M5.2	195, 1600	51±2	19±2	32	16:47:12	16:53:30	...	...	17:02	17:08
2000 Jul 14	X5.7	195	65±2	23±2	42	10:24:23	10:26:51	10:27	9	10:24	10:54
2000 Nov 08	M7.4	171	...	...	...	...	...	...	...	23:28	23:06
2000 Nov 24	X2.3	1600	...	...	...	...	...	...	...	15:13	15:30
2000 Nov 24	X1.8	1600	57±2	15±2	42	21:49:14	21:52:51	21:54:07	76	21:59	22:06
2001 Jan 20	M1.2	1600	...	...	...	...	...	...	...	18:47	19:31
2001 Jan 20	M7.7	1600	...	...	...	...	...	...	...	21:20	21:30
2001 Mar 24	M1.7	171, 1600	80±2	50±2	30	19:37:53	19:55:05	...	...	19:55	20:50
2001 Apr 09	M7.9	171, 1600	63±2	35±2	28	15:25:02	15:31:27	...	...	15:34	15:54
2001 Apr 10	X2.3	171	53±2	2±2	51	05:08:39	05:17:25	05:19	95	05:26	05:30
2001 Apr 11	M2.3	171	76±2	46±2	30	12:58:27	13:07:46			13:26	13:31
2001 Apr 26	M7.8	171, 1600	51±2	5±2	46	13:07:48	13:09:54	13:10:10	16	13:12	13:31
2001 Jun 15	M6.3	195	...	...	...	...	...	...	...	10:13	10:31
2001 Aug 25	X5.3	284	...	...	...	...	...	...	...	16:45	16:50
2001 Oct 19	X1.6	171	...	...	...	...	...	...	...	16:30	16:50
2001 Dec 26	M7.14	1600	...	...	...	...	...	...	...	05:40	05:30
2002 Mar 14	M5.7	171	61±2	26±2	35	01:42:02	01:47:22	01:46	−82	01:50	23:54
2002 Apr 10	M1.6	195	52±2	27±2	25	19:01:55	19:04:03	19:04:15	12	19:07	20:26
2002 Jul 29	M4.7	171, 1600	...	...	...	...	...	...	...	10:44	No
2002 Jul 31	M1.2	171	50±2	1±2	49	19:37:53	01:51:10	01:51:40	30	01:53	No
2002 Oct 22	M1.0	195	85±2	50±2	35	15:32:18	15:33:25	...	...	15:35	No
2002 Oct 25	M1.5	195	...	...	...	...	...	...	...	17:47	18:06
2003 May 29	X1.2	195, 1600	...	...	...	...	...	...	...	01:05	01:27
2003 May 31	M9.3	195	52±2	29±2	23	02:19:03	02:21:54	...	...	02:24	02:30
2003 Jun 11	X1.6	1700	...	...	...	...	...	...	...	20:14	No data
2003 Aug 19	M2.7	171, 195, 1600	70±2	48±2	22	09:49:45	10:00:24	10:02:22	118	10:06	10:30
2003 Oct 24	M7.6	195, 1600	72±2	41±2	31	02:27:56	02:44:58	02:52:20	440	02:54	02:54
2003 Oct 28	X17.2	195, 1600, 284	78±2	22±2	56	11:00:41	11:04:05	11:05	55	11:10	11:30
2004 Nov 10	X2.5	1600	...	...	...	...	...	...	...	02:13	02:26
2004 Dec 30	M2.2	1600	...	...	...	...	...	...	...	10:47	10:57
2005 Jan 15	X2.6	1600	...	...	...	...	...	...	...	23:02	23:06
2005 May 17	M1.8	171	75±2	36±2	39	02:33:37	02:42:46	02:42:50	4	02:39	03:06
2005 Jul 07	M4.9	171, 1600	61±2	18±2	43	16:07:21	16:20:50	...	...	16:29	17:06
2005 Jul 09	M2.8	171, 1600	48±2	19±2	29	21:55:55	22:05:27	...	...	22:06	22:30
2005 Jul 30	X1.3	171	...	...	...	...	...	...	...	06:35	06:50
2005 Sep 17	M9.8	171, 1600	67±2	46±2	21	06:02:15	06:04:53	06:05:40	47	06:05	No

[a] θ_1 and θ_2 refer to the initial and final shear angles, respectively.
[b] t_{EUV1} and t_{EUV2} refer to the time when the initial and final shear angles are measured, respectively.
[c] The time when the impulsive phase stops.

shown in Figure 1*b*. Figures 1*c* and 1*d* show the initial and final brightenings (*white contours*) overlaid on the later postflare loop images showing the postflare loops connecting these brightenings, respectively. The *TRACE* image at the time when the shear change stops overlaid with photospheric magnetic field contours observed by *SOHO* MDI is shown in Figure 1*e*. Figures 1*f* and 1*g* show how we measure the initial and final shear angle.

Type II flares.—We do not see measurable shear motion of the conjugate brightenings, but we see very small ribbon separation in this type of flare (e.g., Figs. 2*a* and 2*b*).

Type III flares.—We do not see shear motion of the conjugate brightenings, nor ribbon separation in these flares. Two examples of type III flares are shown in Figures 2*c*–2*f*.

3.1. *Type I Flares*

3.1.1. *Footpoint Motion in Type I Flares*

In all, 86% (43 out of 50) of the two-ribbon flares we studied show shear motion of the EUV/UV footpoints during the flare, which indicates that this motion is a common feature in two-ribbon flares. This 86% fraction is much larger than the 45% (14 out of 31) fraction reported by Bogachev et al. (2005). They found that 8 of these 14 flares with shear motion show mainly this shear motion, while the other 6 flares show a combination of ribbon separation and shear motion. However, all of our 86% of flares show a combination of ribbon separation and shear motion. Two reasons that may explain this difference are as follows: (1) Data

TABLE 2

TYPE II AND TYPE III FLARES WITHOUT SHEAR MOTION

Date	*GOES* Class	Observed Band(s) (Å)	*GOES* Peak Time (UT)	Ribbon Separation	CME Onset Time (UT)
2001 May 05[a]	M1.0	171, 1600	08:56	Small	No
2001 Aug 05[b]	M1.7	171, 1600	15:31	No	No
2001 Aug 05[b]	M4.9	171, 1600	22:24	No	No
2001 Oct 31[c]	M3.2	171	08:09	No	No
2001 Nov 10[c]	M1.0	1600	00:50	No	No
2001 Dec 29[c]	M1.1	1600	05:45	No	No
2003 Jan 22[a]	M1.2	171	04:44	Small	05:06

[a] Type II flares.
[b] Type IIIA flares.
[c] Type IIIB flares.

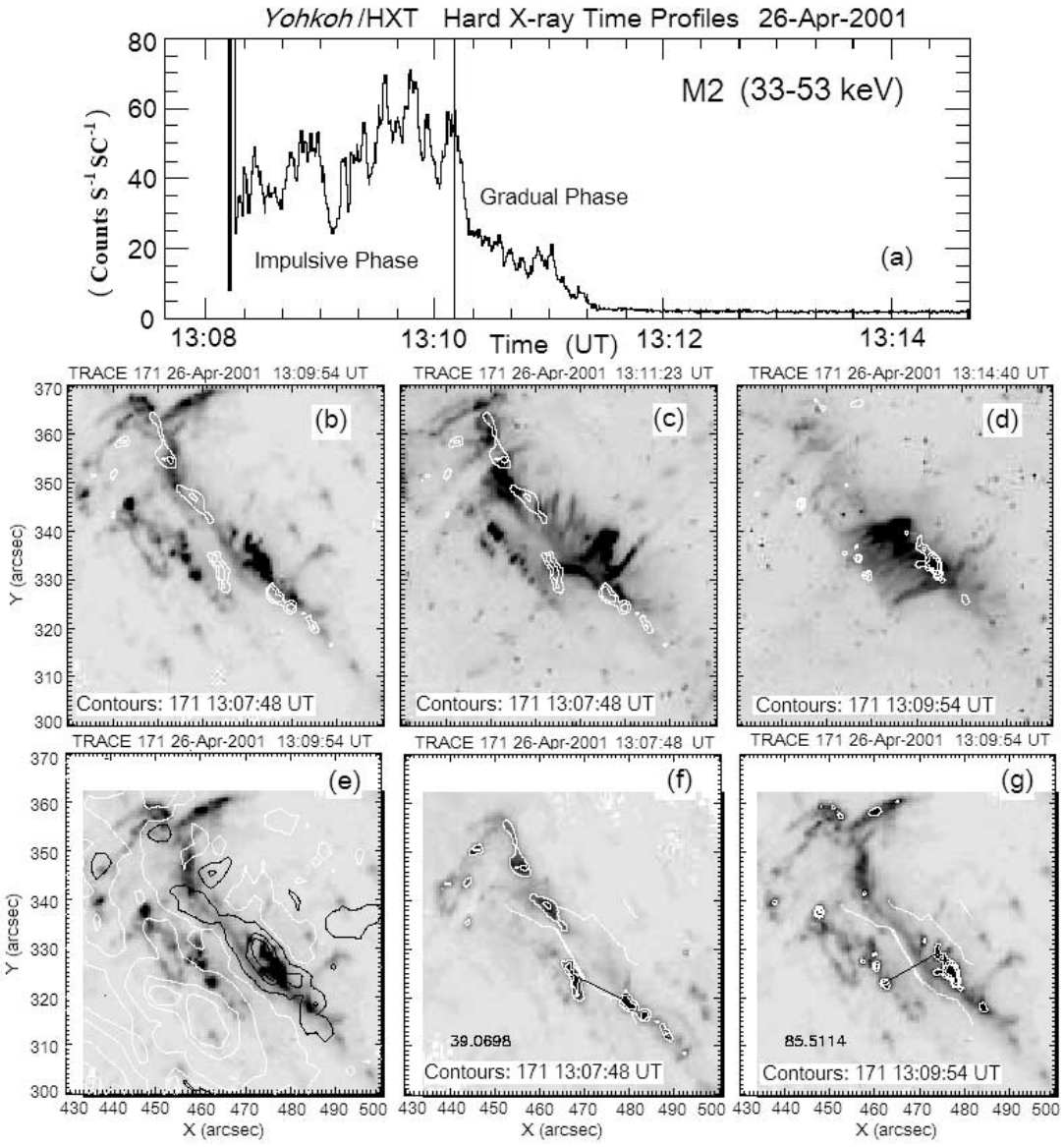

FIG. 1.—Event on 2001 April 26. (*a*) HXR ($E = 33$–53 keV) time profile observed by *Yohkoh* HXT. The end of the impulsive phase is marked as a vertical line. (*b*–*d*) EUV images at 171 Å observed by *TRACE* at different times. (*e*) *TRACE* EUV image overlaid with corresponding photospheric magnetic field (*SOHO* MDI) contours. The black and white contours represent the positive and negative magnetic polarities, respectively. (*f*, *g*) *TRACE* EUV images at different times overlaid with white contours that represent the brightenings. The white lines refer to the magnetic inversion line (MIL, *SOHO* MDI), and the thick white lines represent the simplified MIL. The brightenings connected by the black lines are conjugate footpoints.

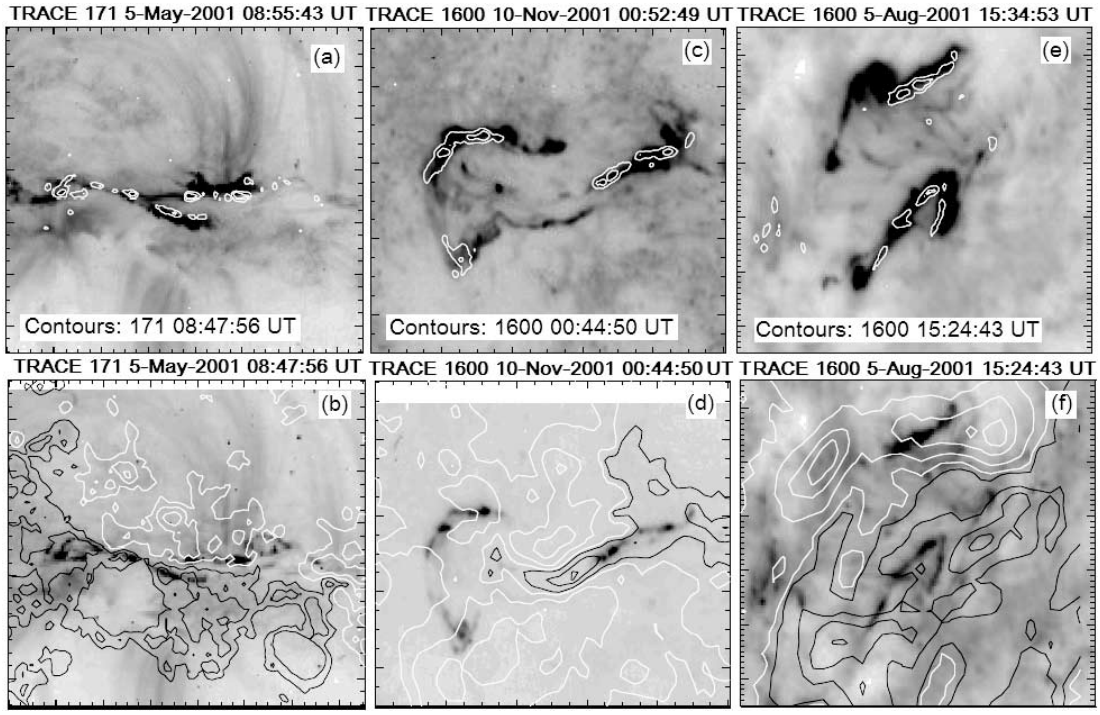

FIG. 2.—Type II and III flares. *Left*: Images for event 2001 May 5, and the FOV is $150'' \times 125''$. (*a*) *TRACE* image at around the *GOES* flare peak time overlaid with white contours representing the bright kernels at the flare onset. (*b*) *TRACE* image at the flare onset overlaid with photospheric magnetic contours. The black and white contours refer to the positive and negative magnetic polarities (*SOHO* MDI), respectively. *Middle*: Similar to the left panels, but for event 2001 November 10, and the FOV is $100'' \times 85''$. *Right:* Similar to the left panels, but for event 2001 August 5, and the FOV is $70'' \times 60''$.

selection criteria are different. All of the flares we selected must have two long and nearly parallel ribbons observed by *TRACE*, which is not required by Bogachev et al. (2005). (2) Bogachev et al. (2005) used HXR data observed by *Yohkoh* HXT ($2.47''$ pixel^{-1}), while we are measuring the EUV/UV footpoints using the much higher spatial resolution ($0.5''$ pixel^{-1}) data observed by *TRACE*.

As mentioned in § 1, there are mainly three types of HXR footpoint motions: ribbon separation, shear motion, and motion in the same direction (Bogachev et al. 2005). In this paper, although we focus our study on the shear motion of EUV/UV footpoints, we have also checked for the other two types of motions, i.e., ribbon separation and motion in the same direction. We have found that all of the 43 type I flares show both ribbon separation and shear motion, and the brightest footpoints in 22 out of the 43 type I flares show "same direction" motion along with the shear motion and ribbon separation. This indicates that a mixture of these three types of motion often exists in two-ribbon eruptive flares.

3.1.2. *Shear Angles of the Footpoints in Type I Flares*

In order to get a quantitative determination of the shear motion of conjugate footpoints, we have selected 24 events out of the 43 type I flares, representing those events for which the MIL information and *TRACE* observations are good enough to (1) represent the magnetic inversion line using a straight line and (2) identify the initial and final conjugate footpoints. The initial and final shear angles of these events have been measured and listed in Table 1. The shear angle is defined as the angle between the line connecting the conjugate footpoints and the line perpendicular to the magnetic inversion line.

We have developed a semiautomatic program to measure the shear angles of these events. The projection effects of events close to the limb have been corrected by moving the source region to the solar disk center in software. The process of measuring the shear angles is described as follows:

1. Inspect and compare all of the EUV/UV images overlaid with magnetic field contours during the flare to select two EUV/UV images. The first image is the one when the initial brightenings (e.g., white contours on Fig. 1*b*) appear, and the second image is the one when the shear change of footpoints stops (e.g., Fig. 1*b*). For those flares without *SOHO* MDI observations, all of the EUV/UV images are shown as contours overlaid on the BBSO Hα image closest in time, and the MIL is indicated by the filament.
2. Select the initial and final conjugate footpoints from the two images. Most events start as two bright kernels appearing on both sides of the MIL. These two bright kernels will be identified as the initial conjugate footpoints if they are subsequently connected by corresponding postflare loops (e.g., Fig. 1*c*). Two long ribbons composed of many bright kernels have been formed by the time the shear motion of the footpoints stops. We choose the brightest brightening pair at the end of shear change as the final conjugate footpoints. Furthermore, the corresponding postflare loops for most of these brightening pairs at this time are roughly parallel to each other (e.g., Fig. 1*d*), which means that the shear angles of most of the brightening pairs are similar.
3. The angle between the line connecting the two conjugate footpoints (black line in Figs. 1*f* and 1*g*) and the simplified magnetic inversion line (thick white line in Figs. 1*f* and 1*g*) is measured using our semiautomatic program. This angle can be measured by clicking the start and end points of the MIL and the two conjugate footpoints on the image. Note that the shear angle is complementary to the angle thus measured.

The various parameters of all type I flares are listed in Table 1. The histogram of event number in terms of the initial and final shear angles (Fig. 3*a*) shows that the initial and final angles in most events are in the range from 50° to 80° and from 15° to 55°,

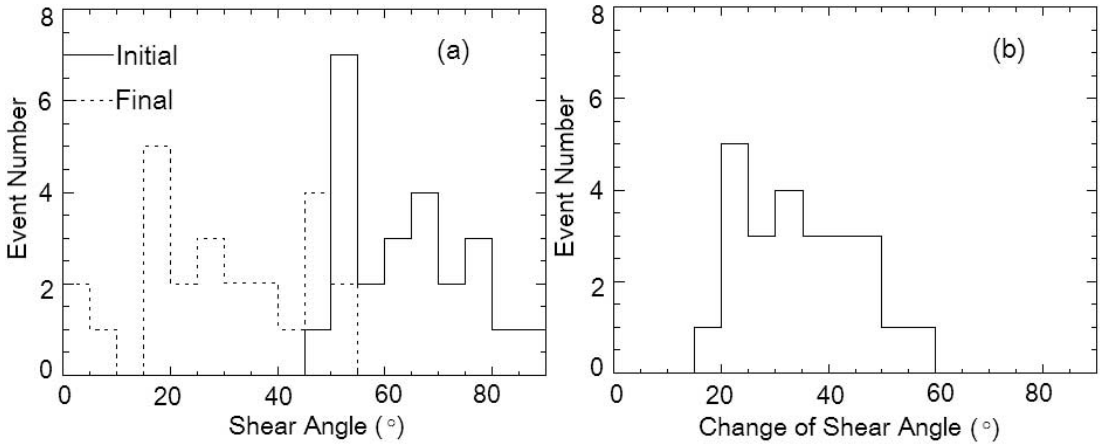

FIG. 3.—Histograms for the 24 type I flares with measured shear angle. (*a*) Histogram of event number in terms of the initial and final shear angles. (*b*) Histogram of event number in terms of the change of shear angle. The bin size in these two histograms is 5°.

respectively. The distribution of the final shear angle may suggest that the magnetic field does not generally relax fully to a potential state (Gibson & Fan 2006b). This is because reconnection under high electrical conductivity approximately conserves the global magnetic helicity, according to Berger & Field (1984). Thus, coronal fields will naturally produce a flux rope, rather than a potential field, as a metastable state (Zhang & Low 2005). It is worth noting here that, due to the uncertainties in our method of measuring shear angle (e.g., we use a simplified straight line to represent the magnetic inversion line), we cannot exclude the possibility that the magnetic field does relax to a fully potential state after the flare for some events, especially those events having final shear angle less than 15°. In order to make sure if the magnetic field relaxes to a fully potential state or not, we should make detailed calculations using the potential magnetic field model, which is beyond the scope of this paper.

Figure 3*b* is the histogram of event number in terms of the change of shear angle, which shows that the change of shear angle is distributed in the range between 15° and 60°.

3.2. *Type II and III Flares*

These types of flares have no obvious shear change of the footpoints. All of these flares have relatively low soft X-ray flux (*GOES* class <M5).

Type II flares (marked as "a" in Table 2) show very small ribbon separation during the flare (e.g., Fig. 2*a*). We found two such events. In both cases, a filament is seen before the flare in both *TRACE* and the Hα images (BBSO). The two ribbons initially appear close to the magnetic inversion line, then move outward very slightly away from the MIL. There is no observable filament activation associated with event 2001 May 5, but a filament eruption is seen to be associated with event 2003 January 22. Both type II flares have single-bipole magnetic field configuration (Fig. 2*b*).

We found five type III events (marked as "b" and "c" in Table 2), in which there is no observed ribbon separation. The brightenings of all type III flares appear at a position far from the magnetic inversion line, and the shear of the conjugate brightenings is very weak at the flare onset. As the flare progresses, the two ribbons may show some expansion along the direction parallel to the inversion line, but there is no motion along the direction perpendicular to the MIL at all throughout the entire flare process (i.e., Figs. 2*c* and 2*e*). Type III flares are divided into two subgroups (i.e., type IIIA and type IIIB marked as "b" and "c" in Table 2, respectively) based on the photospheric magnetic field configuration. The difference between type IIIA and type IIIB flares is that type IIIA flares have a complicated magnetic field configuration (e.g., Fig. 2*d*), whereas type IIIB flares have a simple single-bipole magnetic field configuration (e.g., Fig. 2*f*).

4. EJECTIVE AND CONFINED FLARES

Flares have been categorized in many different ways, but two particular types, the simple-loop (compact or confined) flare and the two-ribbon (dynamic or ejected) flare, may be particularly significant (Pallavicini et al. 1977; Moore et al. 1980; Priest 1981). In compact flares we see brightenings of loops that do not show any apparent expansion, rise, or other kinds of motion. In Hα, the brightened footpoints of the flare stay in the same position until they decay. They do not appear to be associated with filament disruption (which is a characteristic feature of the two-ribbon flares), nor with white-light coronal transients (which are consequences of the filament disruptions; Priest 1981). The two-ribbon flares are much larger and more dramatic than a compact flare and take place near a solar prominence or filament. During the flash phase, two ribbons of Hα emission form, one on each side of the filament (or filament channel), and throughout the main phase the ribbons move apart at 2–10 km s^{-1}. Occasionally, the filament remains intact, although slightly disturbed, but usually it rises and disappears completely (Priest 1981). Following Svestka (1986), the first class of flares are called "confined" flares to emphasize their essential difference from the other classes, and the other class are called "ejective" flares (Machado et al. 1988).

In this section we compare our classification scheme (§ 3) with that of Svestka (1986) and introduce some available models for these flares. We classify those flares having both ribbon separation and corresponding CMEs into the ejective flare category. For some flares we do not find corresponding CMEs from the *SOHO* LASCO CME Catalog, and we call these flares "possibly ejective." Flares having no ribbon separation nor corresponding CMEs are classified into the confined flare category. We regard the flare and CME as associated if the CME onset time (first appearance time at LASCO C2) is within a ±2 hr time window of the flare peak time and the position of the flare lies in the range of the CME span, defined as the position of the CME ± half of the CME width ±15° (Zhang & Golub 2003). If the CME candidate is a halo CME, then the center of the *TRACE* field must lie within 45° of disk center in both longitude and latitude; otherwise, the

latitude of the center position of the *TRACE* field must lie in the range of the CME span, according to Zhang et al. (2002).

4.1. *Ejective or Possibly Ejective Flares*

From Tables 1 and 2 we can see that 36 type I flares plus one type II flare belong to the ejective flare category. For this type of flare, there is now a generally accepted picture for the overall three-dimensional magnetic field and its change during the flare. This standard picture is basically the one proposed by Hirayama (1974), which (with various modifications, refinements, and changes in emphasis) has been adopted by many flare modelers (Moore et al. 1995 and references therein). In this scheme, the flare energy release is driven by the eruption of a magnetic flux rope from the sheared core of a closed bipolar magnetic field (Moore 1988; Forbes 1992). The strong-to-weak shear motion of the footpoints is interpreted as magnetic reconnection progressing from a highly sheared to a less sheared region (Fig. 11 in Paper I). This strong-to-weak shear motion of the footpoints or of the "post-flare" loops is seen in a magnetohydrodynamic (MHD) simulation of the nonlinear development of instabilities of magnetically sheared arcades made by Manchester (2003; see his Fig. 2). MHD simulations of the eruption of a three-dimensional flux rope done by Gibson & Fan (2006b) and Manchester et al. (2004) also show this motion (see their Figs. 5*g*–5*i*).

For the other seven type I flares and one type II flare, the corresponding CME information is uncertain. The CME onset times for all of the flares we studied are listed in the last column of Tables 1 and 2. For two flares the CME information is uncertain because there is a gap in LASCO observations (marked as "No data"). For the other six flares, we do not find corresponding CMEs fitting our criteria. Note that although we do not find corresponding CMEs from the LASCO C2 observations, we cannot say that these flares are not associated with CMEs because the associated CME may be too weak to be detected by the *SOHO* LASCO C2. We call these flares possibly ejective flares because they show ribbon separation, but there is no certain corresponding CME information.

For two out of these eight possibly ejective flares, we see obvious filament eruptions in EUV observations made by *TRACE*. Although the corresponding CME information is uncertain, we suggest that these two possibly ejective flares, similar to ejective flares, may also be caused by the ejective eruption of the sheared core field (Moore et al. 2001). It is worth noting that in this scheme, all or part of the filament (sheared core field) is often seen to erupt in association with a flare. However, according to Gibson & Fan (2006a, 2006b), the degree to which the initially dipped field was filled with filament mass, as well as the location of this mass relative to where the flux rope breaks in two, would then determine whether all, some, or none of the filament would actually be observed to erupt and escape with the CME. If only the lower dips were filled with filament mass, the filament might not show any sign of eruption at all, which may explain why we do not see filament eruption in the other six possibly ejective flares (e.g., event 2001 May 5). Since the flux rope or the envelope of the sheared core field can break in two (Gibson & Fan 2006a, 2006b; Paper I), a weak CME may happen if only a smaller upper part of the flux rope (CME) is ejected, and the larger lower part of the flux rope is left behind. Therefore, these six possibly ejective flares may be caused by partial eruption of the flux rope (or sheared core field).

4.2. *Confined Flares*

It is known that ribbons of large two-ribbon flares separate as a function of time, which can be interpreted by the classical two-dimensional magnetic reconnection model discussed in § 1. However, the separation of ribbons is not universal, and we observed several small two-ribbon flares (i.e., type III flares) that have no ribbon separation at all throughout the entire flare process. The ribbons of these flares are not close together at the flare onset and no strong shear of the footpoints is observed either, which is consistent with the earlier results reported by Tang (1985) and Kurokawa (1989).

We find that all five type III flares belong in the confined category for which no corresponding CMEs have been found from the *SOHO* LASCO observations, and all five of these flares have low soft X-ray peak flux (GOES class <M5). These observations suggest that only a small amount of energy is released in these flares; therefore, there might be very little free energy stored prior to the flare.

In the following we discuss our observations in the context of models for confined flares:

1. *Emerging* (*or evolving*) *flux model*.—According to this model, a (small) confined flare occurs if the new flux appears in a region where no great amount of magnetic energy in excess of potential is stored (Heyvaerts et al. 1977; Shibata et al. 1992). All three type IIIA flares have complicated magnetic field configuration, such as in the flare on 2001 November 10 (e.g., Fig. 2*d*): the negative polarity is surrounded by the positive polarities and the magnetic inversion line is strongly contorted; therefore, this MIL can be treated as two magnetic inversion lines. However, the two type IIIB flares have a single bipolar configuration, and the magnetic inversion line is nearly straight. More than one magnetic inversion line is needed to make this model work. Therefore, this model seems possible for the type IIIA flares but may not fit the type IIIB flares.

2. (*Resistive*) *kink instability*.—When a loop is twisted by more than a critical amount, it becomes kink or resistive kink unstable. If ideal kink occurs, the loop may become contorted and develop current sheets in the nonlinear development. If the resistive kink takes place, one or several current sheets form at which the magnetic energy is dissipated (Sakurai 1976; Priest 1981; Gerrard & Hood 2003). A recent simulation done by Török & Kliem (2005) shows that the kink instability of coronal magnetic flux ropes could drive confined eruptions if the decrease of the magnetic field above the flux rope is not steep enough. For our confined flares, we do not see any observational evidence that supports this model, but we also do not have enough observational evidence to rule out this possibility.

3. *Confined explosion of a sheared core bipole*.—The sheared core field and filament undergo an eruption that is soon arrested within the confines of the closed bipole, and the flare has a correspondingly short duration (Moore et al. 2001). This model predicts that the brightenings at the flare onset are highly sheared and close to the inversion line, while our observations show that the brightenings in the five confined (i.e., type III) flares at the flare onset are weakly sheared and far away from the inversion line (e.g., Fig. 2).

4.3. *An Energy Scale for Two-Ribbon Flares*

Table 3 shows the relationship between the two types of classification for all of the flares we studied using different criteria. From Table 3 we can see that ejective flares almost always show shear change of the footpoints (only 1 counterexample out of 37). There are two flares that show ribbon separation but no shear motion. However, shear motion of the footpoints is always accompanied by ribbon separation.

The eruptive or noneruptive behavior of flares is likely determined by the *relative* amount of free energy ε, i.e., the ratio of

TABLE 3
CLASSIFICATION OF "EJECTIVE" AND "CONFINED" FLARES

Type (Motion)	Ejective (CME)	Possibly Ejective (CME?)	Confined (No CME)
I (RS[a] and SM[b])	36	7	0
II (RS)	1	1	0
III (no motion)	0	0	5

[a] Ribbon separation.
[b] Shear motion.

the magnetic free energy ΔE released in the flare and the energy $\Delta E_{\rm open}$ required to open up the field. For $\varepsilon \geq 1$ sufficient energy is available to produce an eruption, whereas for $\varepsilon \ll 1$ only confined flares are energetically possible. We suggest that this ratio ε also determines the type of footpoint motions that occur within the flare. Figure 4 shows a schematic representation of the flare energy scale sequence of the three types (types I, II, and III) of flares. Type I flares are the most powerful eruptions, which show both shear motion of the footpoints and ribbon separation, and most of these flares are associated with CMEs. This suggests that a large amount of free energy is stored in the corona prior to this type of flare, $\varepsilon \geq 1$. Type II flares are relatively smaller flares, and they only show very small ribbon separation, but no measurable shear change of the footpoints, and only one of the observed type II flares is associated with a CME. These observations may indicate that the free energy stored in the magnetic field in these flares is relatively small, i.e., $\varepsilon < 1$, which causes very small ribbon separation and no obvious shear change of the footpoints. Type III flares show no shear change of the footpoints nor ribbon separation, and no corresponding CMEs. There is for such flares only minor nonpotentiality and thus the energy in the corona prior to eruption is small (Priest & Forbes 2002).

5. TIME DIFFERENCE BETWEEN THE CESSATION OF SHEAR MOTION AND THE END OF IMPULSIVE PHASE IN TYPE I FLARES

We have selected 14 events with good corresponding HXR (*Yohkoh* HXT or *RHESSI*) observations out of the 24 type I flares with measured shear angle, in order to answer the question, could the transition from impulsive to gradual phase be related to the magnetic shear change?

In the impulsive phase of these flares, the HXR and gamma-ray emission rises impulsively, often with many short but intense spikes of emission, each lasting a few seconds to tens of seconds. The end of the impulsive phase in this study is defined as the last peak of the impulsive phase (e.g., the vertical line in Fig. 1*a*). We note that in most events, the time of the end of the impulsive phase is earlier than the *GOES* soft X-ray peak time, which is listed in Table 1. In the gradual phase, the HXR and gamma-ray fluxes start to decay away more or less exponentially with a time constant of minutes (e.g., Fig. 1*a*).

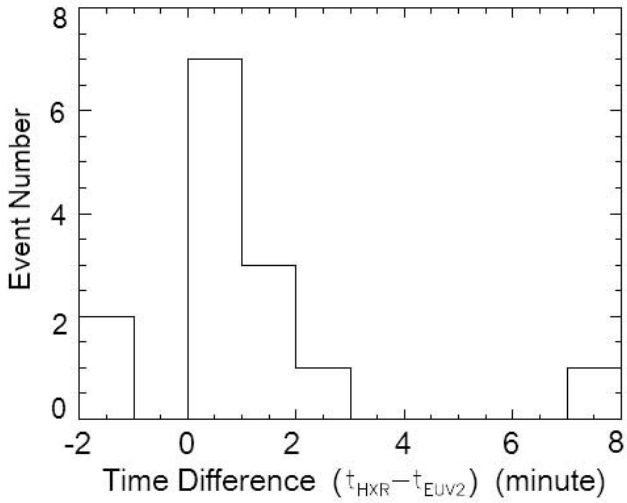

FIG. 5.—Histogram of event number in terms of the time difference between the end of the HXR impulsive phase and the cessation of the change of shear angle in the 14 type I flares with both measured shear angles and corresponding HXR observations. The time bin size is 1 minute.

The histogram of the time difference between the end of the HXR impulsive phase and the cessation of the shear change shows that in most events, the cessation of shear change is 0–2 minutes earlier than the time when the impulsive phase stops (Fig. 5).

This observation indicates that during the impulsive phase magnetic reconnection occurs mainly in the highly sheared region (within the filament channel), but reconnection progresses out to the weakly sheared region (outside the filament channel) during the gradual phase. This result implies that the change from impulsive phase to gradual phase may be related to the magnetic shear change as suggested by Lynch et al. (2004), although the two changes do not happen at exactly the same time. The observation also indicates that the splitting of the sheared envelope of the highly sheared core field happens near the end of the impulsive phase in most cases, since the cessation of shear change may be interpreted as this splitting of the sheared envelope (Paper I).

6. SUMMARY

We have, for the first time, carried out a statistical study of shear motion of the UV/EUV footpoints in a large sample (50) of well-observed X and M class two-ribbon flares, observed by *TRACE* in 1998–2005. These flares are classified into three groups: type I flares, which show shear motion of footpoints and ribbon separation; type II flares, which show ribbon separation but no measurable shear motion of footpoints; and type III flares, which

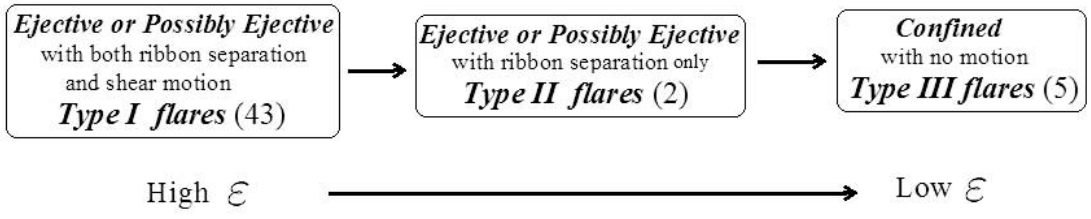

FIG. 4.—Schematic representation of the flare energy scale indicating the type of flare footpoint motions. Here "ε" refers to the relative amount of magnetic free energy in the corona prior to the flare.

show no shear motion of the footpoints or ribbon separation. We also compared our classification with the traditional classification of ejective and confined flares (Svestka 1986). Our results can be summarized as follows:

1. Our study shows that 86% (43 out of 50) of the flares belong to type I, and all type I flares (ejective or possibly ejective) show obvious ribbon separation during the flare. This 86% fraction is much larger than the 45% (14 out of 31) fraction reported by Bogachev et al. (2005). Our observations indicate that both shear motion of conjugate footpoints and ribbon separation are common features in two-ribbon flares. These flares may be interpreted with the well-accepted standard picture of two-ribbon eruptive flares, which is the (whole or partial) eruption of a magnetic flux rope from the sheared core of a closed bipolar magnetic field (Moore et al. 1995 and references therein). A detailed description of this standard model and the interpretation of shear motion of footpoints are given in Paper I.

2. Ejective flares (which have ribbon separation and corresponding CMEs) almost always show shear change of the footpoints (only 1 counterexample out of 37). There are two flares that show ribbon separation but no shear motion. However, shear motion of the footpoints is always accompanied by ribbon separation, which is not consistent with the result reported by Bogachev et al. (2005), who found that 8 out of the 31 flares show mainly shear motion.

3. The initial and final angles of the footpoints in 24 type I flares have been measured, and they are mainly distributed in the range from 50° to 80° and from 15° to 55°, respectively, in most events. This result may indicate that the magnetic field relaxes toward, but does not generally reach, a fully potential state. However, we cannot exclude the possibility that the magnetic field does relax to a fully potential state after the flare for some events, especially those events having final shear angle less than 15°, due to the uncertainties in our measurements of the shear angle. The *change* of shear angle is in the range between 15° and 60°. This measurement of the distributions of the initial and final shear angles may provide some constraints on three-dimensional magnetic reconnection models for solar eruptions.

4. Some flares show no shear change of the conjugate footpoints during the flare. These flares have either no obvious ribbon separation (five type III flares) or very small ribbon separation (two type II flares). Similar to type I flares, type II flares may also be driven by the (whole or partial) eruption of a magnetic flux rope from the sheared core of a closed bipolar magnetic field, but we speculate that these are partial eruptions involving a relatively small amount of axial magnetic flux. The brightenings of type III flares appear at a position far from the magnetic inversion line at the flare onset, and no ribbon separation is observed during the flare. These flares belong to the confined flare category. Our observations in the context of several models for confined flares are discussed in § 4.2.

5. The cessation of shear change is 0–2 minutes earlier than the end of the impulsive phase in 10 out of the 14 events with measured shear angle and corresponding HXR observations. This provides a positive answer to our hypothesis, namely, that the change from impulsive to gradual phase appears to be related to the magnetic shear change.

We acknowledge the referee for his or her valuable suggestions to improve this paper. Y. N. S. sincerely thanks Spiro Antiochos, Ed Deluca, Jun Lin, Mark Weber, Guangli Huang, and Judith Karpen for fruitful discussions and valuable suggestions. The authors wish to thank the teams of *TRACE*, *SOHO* MDI, NJIT BBSO, *Yohkoh*/HXT, and *RHESSI* for providing the valuable data. The authors would like to thank all those who put tremendous efforts into generating these catalogs: the *TRACE* Flare Catalog (footnote 3), kindly provided by the Solar and Stellar X-Ray Group at the Smithsonian Astrophysical Observatory; the *Yohkoh* Flare Catalog (footnote 5), kindly provided by J. Sato et al.; and the *GOES* Flare Catalog (footnote 4), kindly provided by the Space Environment Center, National Oceanic and Atmospheric Administration. The CME Catalog (footnote 6) is generated and maintained at the CDAW Data Center by NASA and the Catholic University of America in cooperation with the Naval Research Laboratory. *SOHO* is a project of international cooperation between ESA and NASA. The *TRACE* analysis was supported at Smithsonian Astrophysics Observatory (SAO) by a contract from Lockheed Martin. Y. N. S. was also supported by an SAO Predoctoral Fellowship, the NSFC projects with 10333030 and 10273025, and "973" program with 2006CB806302.

REFERENCES

Berger, M. A., & Field, G. B. 1984, J. Fluid Mech., 147, 133
Bogachev, S. A., Somov, B. V., Kosugi, T., & Sakao, T. 2005, ApJ, 630, 561
Forbes, T. G. 1992, in Eruptive Solar Flares, ed. Z. Svestka, B. V. Jackson, & M. E. Machado (Berlin: Springer), 79
Gerrard, C. L., & Hood, A. W. 2003, Sol. Phys., 214, 151
Gibson, S. E., & Fan, Y. 2006a, ApJ, 637, L65
———. 2006b, J. Geophys. Res., in press
Handy, B. N., et al. 1999, Sol. Phys., 187, 229
Heyvaerts, J., Priest, E. R., & Rust, D. M. 1977, ApJ, 216, 123
Hirayama, T. 1974, Sol. Phys., 34, 323
Ji, H. S., Huang, G. L., Wang, H. M., Zhou, T. H., Li, Y. P., Zhang, Y. A., & Song, M. T. 2006, ApJ, 636, L173
Kosugi, T., et al. 1991, Sol. Phys., 136, 17
Kurokawa, H. 1989, Space Sci. Rev., 51, 49
Lin, R. P., et al. 2002, Sol. Phys., 210, 3
Lynch, B. J., Antiochos, S. K., MacNeice, P. J., Zurbuchen, T. H., & Fisk, L. A. 2004, ApJ, 617, 589
Machado, M. E., Moore, R. L., Hernandez, A. M., Rovira, M. G., Hagyard, M. J., & Smith, J. B. 1988, ApJ, 326, 425
Manchester, W. 2003, J. Geophys. Res., 108, 1162
Manchester, W., IV, Gombosi, T., DeZeeuw, D., & Fan, Y. 2004, ApJ, 610, 588
Moore, R., et al. 1980, in Solar Flares: A Monograph from Skylab Solar Workshop II, ed. P. Sturrock (Boulder: Colorado Assoc. Univ. Press), 341
Moore, R. L. 1988, ApJ, 324, 1132
Moore, R. L., LaRosa, T. N., & Orwig, L. E. 1995, ApJ, 438, 985
Moore, R. L., Sterling, A. C., Hudson, H. S., & Lemen, J. R. 2001, ApJ, 552, 833
Pallavicini, R., Serio, S., & Vaiana, G. S. 1977, ApJ, 216, 108
Priest, E. R. 1981, Solar Flare Magnetohydrodynamics (New York: Gordon & Breach)
Priest, E. R., & Forbes, T. G. 2002, A&A Rev., 10, 313
Qiu, J., Lee, J., & Gary, D. E. 2004, ApJ, 603, 335
Sakurai, T. 1976, PASJ, 28, 177
Shibata, K., Nozawa, S., & Matsumoto, R. 1992, PASJ, 44, 265
Su, Y. N., Golub, L., Van Ballegooijen, A. A., & Gros, M. 2006, Sol. Phys., 236, 325 (Paper I)
Svestka, Z. 1986, in The Lower Atmosphere of Solar Flares, ed. D. F. Neidig (Tucson: Univ. Arizona Press), 332
Svestka, Z., & Cliver, E. W. 1992, in Eruptive Solar Flares, ed. Z. Svestka, B. V. Jackson, & M. E. Machado (New York: Springer), 1
Tandberg-Hanssen, E., & Emslie, A. G. 1988, The Physics of Solar Flares (Cambridge: Cambridge Univ. Press)
Tang, F. 1985, Sol. Phys., 102, 131
Török, T., & Kliem, B. 2005, ApJ, 630, L97
Zhang, M., & Golub, L. 2003, ApJ, 595, 1251
Zhang, M., Golub, L., Deluca, E., & Burkepile, J. 2002, ApJ, 574, L97
Zhang, M., & Low, B. C. 2005, ARA&A, 43, 103